Chinese Chemical Letters 34 (2023) 107905

Contents lists available at ScienceDirect

Chinese Chemical Letters

journal homepage: www.elsevier.com/locate/cclet

Oxygen promoted hydrogen production from formaldehyde reforming with oxide-derived Cu nanowires at room temperature

Yutong Wu[a], Chuangwei Liu[a], Yinglei Liu[a], Gaowu Qin[b], Song Li[a,b,*]

[a] Key Lab for Anisotropy and Texture of Materials (MoE), School of Materials Science and Engineering, Northeastern University, Shenyang 110819, China
[b] Institute for Frontier Technologies of Low-Carbon Steelmaking, Shenyang 110819, China

ARTICLE INFO

Article history:
Received 14 June 2022
Revised 26 September 2022
Accepted 13 October 2022
Available online 17 October 2022

Keywords:
Hydrogen production
Oxide-derived Cu
Dynamic chemical modulation
Reforming formaldehyde
Monolithic catalyst

ABSTRACT

This work demonstrates a two-step method to produce oxide-derived Cu nanowires on Cu mesh surface to offer a monolithic catalyst that outstandingly improves the hydrogen production from reforming formaldehyde and water under ambient conditions. Our results not only reveal that the special oxide-derived nanostructure can significantly improve the formaldehyde reforming performance of Cu, but also display that the hydrogen production has a linear relationship with oxygen pressure. Specially, a maximum of 36 times increment in hydrogen generation rate is observed than that without oxygen during the reaction. Density functional theory calculations show that the formaldehyde molecule is adsorbed on Cu surface only when the adsorbed oxygen is in adjacency, and hydrogen release process is the rate-determining step. This work highlights that the activity of deliberately synthesized catalyst can further be promoted by dynamic chemical modulation of surface states during working.

Hydrogen (H_2) has been considered as an ideal energy carrier due to its high energy density (120–140 MJ/kg), clean, and sustainability [1–3]. Widespread use of hydrogen is partially hampered by its distribution since storage and transportation typically requires high pressure and cryogenic conditions. Materials-based hydrogen storage, *viz.* storing hydrogen in compounds such as ammonia borane [4], formic acid [5], formaldehyde [6–8], and hydrides [9], avoids high pressures and low temperatures and more importantly, features higher capacity. Among those potential carriers, inexpensive formaldehyde (HCHO) has many outstanding advantages for it generate hydrogen by spontaneous reforming at room temperature [10]. Although some noble-metal complex catalysts hold amazing formaldehyde reforming performance, the high cost limits their industrial application. Therefore, it is important to synthesize non-precious metal catalysts for reforming formaldehyde under ambient conditions.

Among numerous non-precious metal catalysts, Cu-based nanomaterials are considered as an attractive candidate due to their unique electronic structure and the capability for efficient catalytic dehydrogenation [11,12]. In the past decades, they were developed and used to catalyze formaldehyde conversion in electrochemistry [13,14], gas-phase [12,15], and liquid-phase [2,16,17]. To achieve highly-efficient catalysts, geometry and local electronic structure of active centers are tailored based on structure-property relationships, forming various fabrication strategies to control the particle size and composition [18,19], exposing facets [19], chemical ordering [20], and metal-support interfaces [21,22]. Previous study indicated that formaldehyde was a structure-sensitive molecule, and the conversion temperature on the nanofiber octahedral molecular sieve surface was significantly lower than that on the nanoparticle structure [7]. Therefore, the preparation of nanowire-structured catalyst is a good strategy for formaldehyde dehydrogenation. Recently, the oxide-derived Cu catalysts have attracted much attention due to their finer grains, higher grain boundary density, and superior catalytic performance compared to direct synthesized Cu catalysts [23–26]. Some reports suggest that Cu^+ and residual subsurface oxygen in oxide-derived Cu may tune the surface binding energy, alter reaction pathway, which can significantly improve the catalytic performance [27]. Based on the above studies, it would be a feasible strategy to design an oxide-derived Cu catalyst with nanowire structure for boosting hydrogen production from formaldehyde aqueous reforming.

Herein, we successfully prepare high-density Cu nanowires (NWs) by the electrochemical reduction of CuO NWs, which generate from the oxidation of Cu wire mesh. The oxide-derived Cu NWs is firstly applied to produce hydrogen from formaldehyde/water at ambient conditions (Fig. S1 in Supporting information). High-density nanowire structure and finer grains are beneficial to the conversion of reactants and diffusion of products, while such self-

* Corresponding author.
E-mail address: lis@atm.neu.edu.cn (S. Li).

https://doi.org/10.1016/j.cclet.2022.107905
1001-8417/

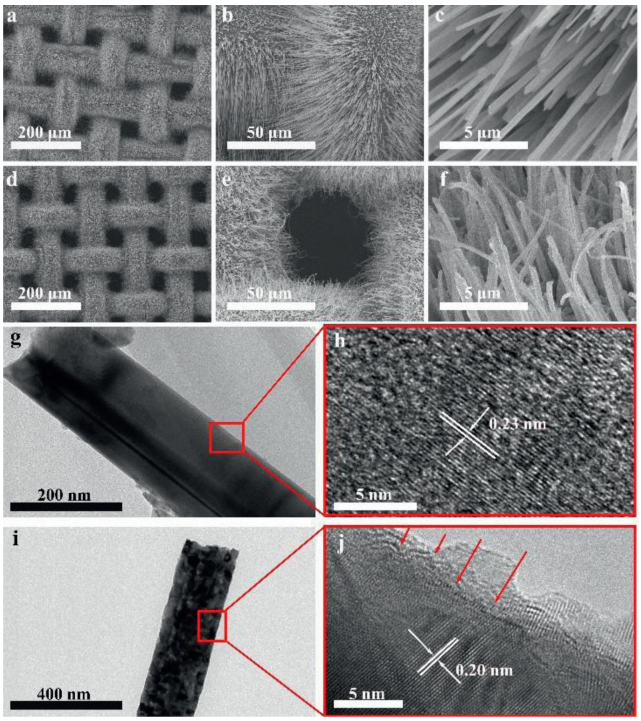

Fig. 1. SEM images of Cu mesh covered by oxide nanowires on the surface, obtained *via* thermal oxidation in air at 600 °C for 4 h (a-c). SEM images of CuNWs obtained after electrochemical reduction at −0.4 V *vs.* RHE (d-f). TEM images of CuO NWs (g, h). TEM images of Cu NWs (i, j).

supported Cu mesh provides convenience for the subsequent separation of catalyst and product. We demonstrate that the catalytic activity of Cu could be significantly enhanced with presence of oxygen. The rate of hydrogen generation is increased by purging oxygen into the reaction. We reveal that the gaseous oxygen activates copper surface *via* forming positively charged Cu sites. This research demonstrates a simple and effective strategy to tune catalytic activities of metal catalysts by dynamic activation.

The SEM morphologies of samples before and after electroreduction are presented in Figs. 1a-f. The Cu mesh surface is completely covered by high density of CuO NW arrays after thermal oxidation at 600 °C in air. Typical diameter of the prepared CuO NWs is about 230 nm, with the length of about 40 μm. TEM observations confirm that the NWs are predominately CuO (Figs. 1g and h). Minor Cu_2O phase exists between the CuO NWs and the Cu woven mesh, which agrees well with the XRD results (Fig. S2 in Supporting information) and follows the Gibbs' phase rule. The high compressive stress in the Cu_2O overlayer drives the NWs growth on Cu surface [28,29]. The lattice fringes with an interplanar lattice spacing of 0.23 nm correspond to the CuO (111) atomic planes (Fig. 1h). Then the oxide NWs are electro-reduced to metallic Cu NWs at −0.4 V (*vs.* RHE). Due to the volume shrinkage during the conversion, the resulting Cu NWs tend to curve [30], as shown in Figs. 1d-f. The magnified TEM image (Fig. 1i) shows that the NWs are rougher after redox and composed of fine Cu nanocrystals, which explains the broadening of the diffraction peaks of the NW arrays (Fig. S2 in Supporting information). In Fig. 1j, many step structures appear at the edge of NW and the crystal lattice distances of 0.2 nm correspond to Cu (111) plane. In addition, monolithic catalysts attached to Cu meshes can be advantageous to trigger or stop reactions by simply inserting or taking out the mesh, allowing for an "on-off" feature [31].

X-ray photoelectron spectroscopy (XPS) is performed to further analyze Cu NWs and CuO NWs samples. As shown in Fig. 2a, the

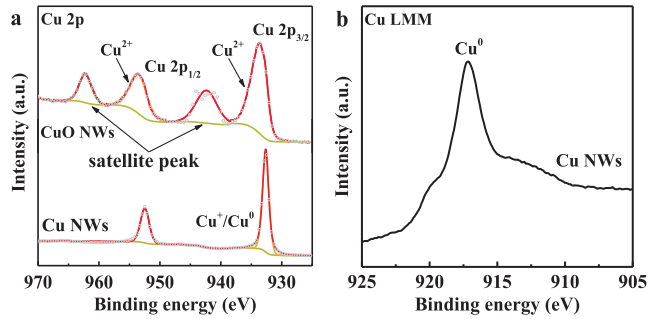

Fig. 2. (a) Cu 2p XPS spectra of Cu NWs and CuO NWs. (b) Cu LMM Auger spectrum of Cu NWs.

Cu $2p_{3/2}$ and Cu $2p_{1/2}$ peaks of CuO NWs around 933.69 eV and 953.55 eV are assigned to Cu^{2+} [32]. Additionally, there are two typical satellite peaks of Cu^{2+} at 942.43 eV and 962.22 eV, indicating the surface of CuO NWs has been completely oxidized. On the electro-reduced Cu NWs sample, two weak peaks at 932.63 eV and 952.47 eV can be assigned to Cu^0 or Cu^+ [33]. Therefore, Cu LMM Auger spectra surface state analysis is performed in Fig. 2b. The peak at 917.12 eV can be assigned to Cu^0 [34]. Combining with the XRD results, CuO is reduced to metallic Cu after electrochemical reduction.

Then, the H_2 production performance on Cu mesh and Cu NWs with and without the presence of oxygen is studied in HCHO (2 mol/L) and KOH (1 mol/L) aqueous solution at ambient conditions. As shown in Fig. 3a, the Cu NWs outperforms the bare Cu mesh in catalytic activity. Hydrogen production is proportional to time with the use of Cu mesh and CuNWs, indicating a uniform hydrogen production rate. Interestingly, it is found that the introduction of different gasses into solution have a great effect on the hydrogen production. The H_2 production performance is improved when O_2 is introduced into the solution, while almost no H_2 is detected under the Ar condition. More importantly, the H_2 yield over Cu NW catalyst is 10 mL in 60 min, nearly 12 times higher than that of pure Cu mesh in the presence of oxygen injection. The large specific surface area of the NW nanostructure and its abundant grain boundaries contribute to the activity by providing more active sites [30]. The H_2 generation rate increases almost linearly with the amounts of the CuNWs mesh (Fig. 3b). As shown in Table S1 (Supporting information), the TOF of Cu NWs is higher than some precious metal catalysts. Considering that the metallic wire of ~50 μm diameter contributes most of the mass, the activity of the Cu NWs monolith in this work is good.

It is well known that the solution can have significant effect on the kinetics of catalytic performance [10]. We investigate the H_2 production of Cu NWs with the presence of oxygen under different concentrations of HCHO and KOH, respectively, and the results are shown in Figs. 3c and d. Negligible change in the H_2 generation rates is observed when the HCHO concentrations are varied between 1.0 mol/L and 2.5 mol/L (Fig. 3c), and the highest rate is obtained in 2.0 mol/L. While, the H_2 generation rate has an obviously vibration under different KOH concentrations (Fig. 3d). The reaction rate increases as the concentrations of KOH change from 0.1 mol/L to 1 mol/L, and then decreases in a more basic solution. Highly alkaline condition promotes Cannizzaro reaction that reforms aldehyde and water into methanol and formic acid ($HCHO + H_2O \rightarrow CH_3OH + COOH$) as competing process [35]. Thus the rates of H_2 generation are decreased at KOH concentration higher than 1.0 mol/L. From the above results, 2 mol/L HCHO and 1 mol/L KOH are viewed as the best reaction conditions.

The above experimental results indicate that the introduction of different gasses into the solution have a large effect on the H_2

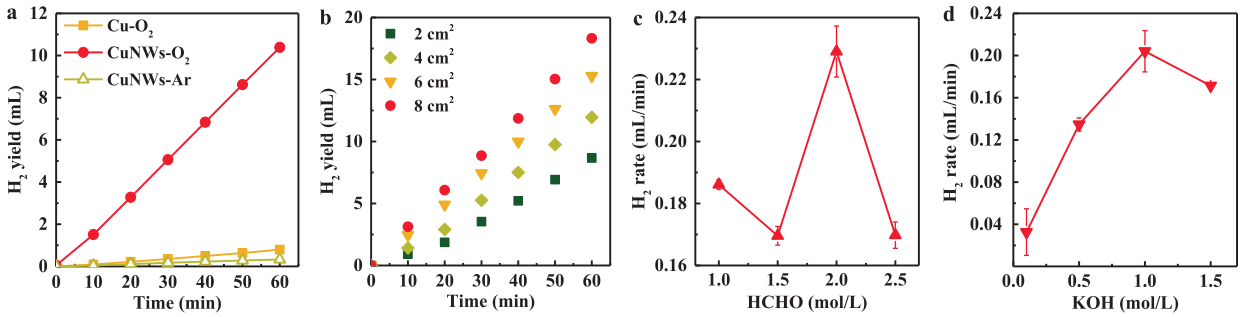

Fig. 3. (a) H_2 evolution from HCHO aqueous solution in presence of the Cu NWs and bare Cu meshes. The concentration of HCHO and KOH are 2 mol/L and 1 mol/L, respectively. (b) H_2 yield with different amounts of Cu NWs mesh. (c) H_2 generation rate in different concentrations of HCHO. (d) H_2 generation rate in 2 mol/L HCHO solution as function of KOH concentration. Area of woven mesh: 4 cm^2. All reactions were performed under a gas flow rate of 15 mL/min.

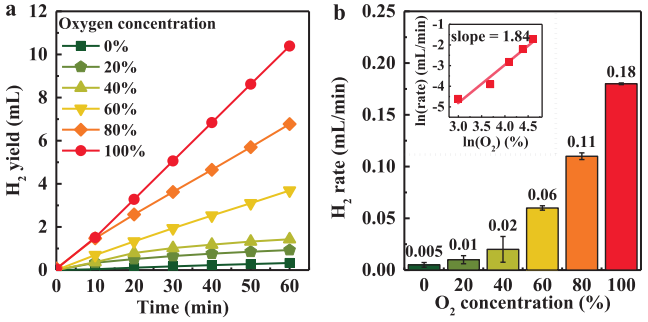

Fig. 4. (a) H_2 evolution over Cu NWs under different oxygen concentrations. (b) Average H_2 generation rate corresponding to (a). Double logarithmic plots of the initial hydrogen evolution rate again oxygen concentration at room temperature (b insert).

production. Therefore, we investigate the role of O_2 partial pressure on the H_2 production performance of HCHO reforming, and the results are summarized in Fig. 4a. The curve displays that the amount of H_2 production increases with increasing oxygen concentration, and the H_2 generation rate is 0.005 mL/min at Ar saturated solution. In other words, negligible amount of H_2 evolved on Cu NWs surface in absence of oxygen. In addition, the rate of hydrogen generation (Fig. 4b) clearly shows the correlation between oxygen and hydrogen evolution, *i.e.*, higher partial pressure of oxygen leads to faster H_2 production, suggesting that O_2 enhances the catalytic activity of Cu NWs. The maximum rate of H_2 in oxygen-rich condition is 0.18 mL/min, which is nearly 36 times larger than that without oxygen. Next, the hydrogen evolution rate over Cu NWs obeys a parabolic correlation with oxygen concentration, and a fitting linear dependency with slope of 1.84 is obtained from double logarithmic plots of the initial reaction rate *vs.* oxygen concentration (Fig. 4b, insert). A positive slope indicates that the activation of oxygen and conversion to reactive oxygen species are the key step limiting the reaction rate. The reactivity of Cu catalyst highly depends on valency and local electronic structure because adsorption of reactive intermediates proceeds *via* electron hybridization. For example, metallic Cu is highly active for catalyzing propylene epoxidation, but its activity is normally suppressed by the oxide layer formed at the catalyst surface in oxidative environment. By illuminating visible light, Linic *et al.* found a steady activity and selectivity of Cu nanoparticles for epoxidation due to light-induced reduction [36]. Also, metallic Cu showed higher catalytic activity than Cu_2O in hydrogen production from *N,N*-dimethylformamide (DMF) and water [37]. It has been previously shown that the reforming of HCHO/H_2O over d^{10} elements can only proceed *via* the oxidized state rather than the corresponding metal [8,10,38], but maintaining the oxidized state is difficult because copper oxide can be easily reduced by formaldehyde. In this work, we deduce that purging oxygen into the reaction creates an electron-deficient state for Cu by extracting electrons from Cu surface and in turn forms an oxide layer [39]. Based upon the correlation between oxygen concentration and rate of H_2 generation (Fig. 4b), these *in-situ* oxidized Cu atoms are catalytically active for the formation of H_2. *In-situ* surface modification has also been found effective in enhancing catalytic performance in different systems. For example, the catalytic activity of Ru/TiO_2 for converting *p*-cresol to toluene was promoted by introducing molecular N_2 into the reaction, and the positive effect was attributed to the formation of hydrogenated nitrogen species on the ruthenium metal surface [40]. The catalytic oxidation of methane into CH_3OH is promoted by introducing water that favors formation of methoxy groups ($^*CH_3O$) [41].

To elucidate the crucial role of oxygen on activating Cu, we further compared the catalytic performance of CuO NWs and Cu NWs under Ar saturate (Fig. 5a) and oxygen saturated (Fig. 5b) conditions, respectively. As shown in Fig. 5a, in the initial 20 min, H_2 generation rate over CuO is much higher than Cu NWs in the absence of O_2. The reactivity over CuO then drops quickly after 20 min and nearly stops after 40 min, and the color of the CuO mesh simultaneously turns from dark brown to red. XRD analysis (Fig. 5c) shows that both CuO and Cu_2O are completely reduced to metallic Cu. And the newly formed Cu is comprised of fine crystal grains, revealed by broader diffraction peaks. These findings indicate that copper oxides are highly active but not stable over the course of hydrogen evolution due to reduction by formaldehyde [42]. For metallic Cu NWs, the reactivity also declines and diminishes quickly, which is associated with the thin copper oxide layer on NWs being quickly reduced to Cu which has no catalytic effect.

The performance of Cu NWs and CuO NWs for H_2 production with the presence of O_2 is shown in Fig. 5b. An induction period exists for both of CuO NWs and Cu NWs to start the hydrogen production. For metallic Cu NWs, the H_2 generation rate peaks after 20 min. In contrast, the oxide catalyst exhibits a longer induction period before reaching a maximum and then diminishes rapidly. We thus infer that the active sites are metallic Cu with adsorbed oxygen. Since copper oxide must be reduced first to Cu, a longer silent period is therefore required. To verify the reasoning, the time taken to reach the highest H_2 generating rate is recorded as a function of oxygen partial pressure (Fig. S3 in Supporting information). It is found that the period increases linearly with the oxygen partial pressure after 40% for the reduction process to Cu is delayed by the dioxygen. The higher O_2 partial pressure, the more time is needed to obtain the clean surface of metallic Cu with adsorbed oxygen. The H_2 generation rate over CuO NWs catalyst decreases to the same to metallic Cu after 70 min when CuO is entirely reduced to Cu, confirmed by that the two starting materials reach same level of activity. In each case, O_2 plays a role in activating in-

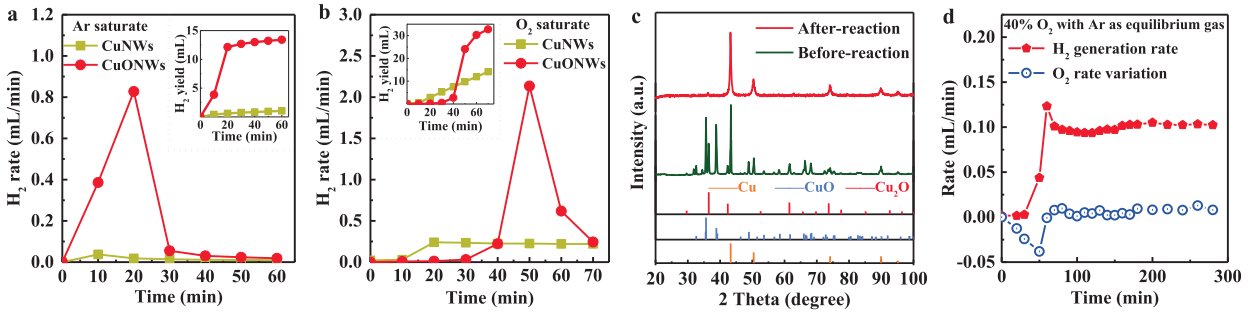

Fig. 5. The performance of nanostructured CuO NWs and Cu NWs catalysts for H_2 generation in the Ar saturate condition (a), and in the O_2 saturate condition (b). Rate of H_2 generation with inset showing the total volume of H_2. The flow rate in (a, b and d) is 15 mL/min. The XRD patterns of CuO NWs catalyst before and after the reaction in the absence of O_2 (c). H_2 generation rate and change in O_2 concentration in Ar flow with 40% O_2 over Cu NWs (d).

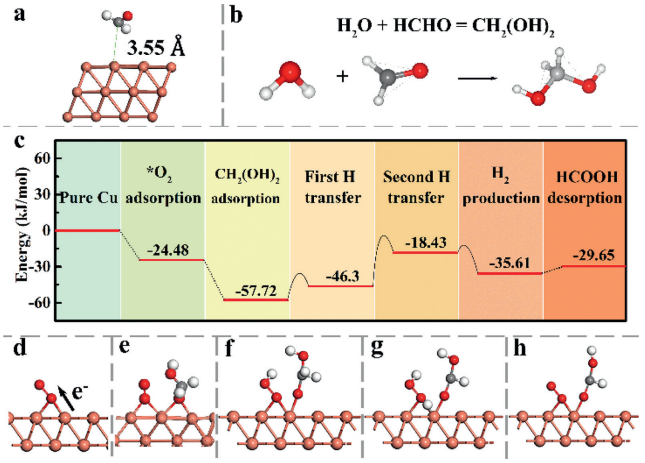

Fig. 6. (a) On bare metallic Cu, no effective adsorption of formaldehyde is formed. (b) The interaction between HCHO and H_2O. (c) Energy diagram of formaldehyde/water reforming process on Cu NWs surface, and (d-h) intermediates of each step.

ert Cu for hydrogen production from the formaldehyde/water system. To further prove the promoting role of oxygen, the rate of H_2 generation and changes of O_2 flow rate are monitored under an oxygen partial pressure of 0.4 (Ar as equilibrium gas) using Cu NWs as the catalyst (Fig. 5d). A decrease in oxygen concentration at the initial stage, due to oxygen absorption by Cu forming surface oxides, is observed along with an abrupt increase in H_2 generation. After that period, the O_2 flow rate remains almost steady, indicating that O_2 is not consumed during the dehydrogenation reaction. To evaluate the cyclic stability of Cu NWs, 4 cm^2 of Cu NWs mesh are taken for H_2 production reaction under optimal conditions for 1 h, and then, the sample is recovered for repeating the above experiment. Fig. S4 (Supporting information) shows that H_2 production experiment is repeated for 8 cycles, and the rate of H_2 production remains a steady state, indicating a good cyclic stability of Cu NWs.

Density functional theory (DFT) calculations are carried out to elucidate the mechanism of activating inert Cu by oxygen adsorption. The (111) surface is of highest percentage in the polycrystals of IB metals and the most thermodynamically stable under the reaction process [42,43]. As shown in Fig. 6a, the distance between pure Cu (111) surface and formaldehyde is 3.55 Å, meaning that formaldehyde could not be adsorbed on the Cu surface [44]. In another word, pure Cu surface is inert for the formaldehyde, making the formaldehyde adsorption the rate determining step of the hydrogen generation reaction.

In aqueous solution, formaldehyde is transformed to hydroxymethanolate ($CH_2(OH)_2$) (Fig. 6b) [38]. After oxygen is chemisorbed on the surface, Cu is activated to capture formaldehyde derivatives and the chemisorption is exothermic (Fig. 6c). The reaction starts with the chemisorption of oxygen on the Cu (111) surface at the bridge site, forming $O_2^{\bullet-}$ radicals by one electron transfer process from the Cu 3d orbital to the empty π^* orbital of O_2 [45]. As a consequence, the chemisorption of oxygen changes the valence of Cu from Cu^0 to Cu^+ (Fig. 6d). In a previous study on the activation of C=O bonds in formaldehyde by Cu^+ in zeolites, electron pair donation from carbonyl oxygen to the metal cation was suggested to be responsible for bonding between the C=O and the cation [46]. Therefore, formaldehyde molecules are difficult to land on surface of metallic Cu due to the lack of empty orbit to accept the pair. Extracting electrons by oxygen endows Cu with the capability of capturing the formaldehyde. The O–H bond in the $HOCH_2OH$ intermediate is cleaved into H^+ and $HOCH_2O^-$ by the activated Cu surface (Fig. 6e). The cleaved H^+ is coupled to adsorbed $^*O_2^{\bullet-}$ forming $^*OOH$, and the $HOCH_2O^-$ is adsorbed on the adjacent Cu^+ site *via* the C=O bond that is not possible for bare metallic Cu (Fig. 6f). Subsequently, $OHCHO^-$ is formed by cleaving C–H bond and releasing $H^{\cdot}$ to Cu site with an estimated activation energy of 27.87 kJ/mol, making it the rate-determining step of the reforming reaction (Fig. 6g). Since the interaction of $^*OOH$ and $H^{\cdot}$ can react easily, H_2 is generated easily (−17.18 kJ/mol) (Fig. 6h) [8,10,45]. Finally, formic acid is desorbed from the Cu surface, and the active Cu site is recovered. Chemisorption of oxygen on Cu surface provides conducive conditions to reforming formaldehyde and water [47]. As we know, the solvation influences catalytic process by a field effect on dipolar reaction intermediate, changing the proton donor for the electron transferred during the reaction. Especially, alkali metal cations (K^+) can stabilize reaction intermediates and decease the kinetic barrier by electrostatic interactions with dipolar intermediates, thereby increasing the formaldehyde reforming process.

Both of experiments and calculations prove that introducing oxygen is necessary because the $O_2^{\bullet-}$ species activate Cu sites. Similar promotion effect of dioxygen was previously observed on MgO supported Ag, where synergistic effect between the metal and the oxide support was attributed to [8,10]. However, in this work, all the cycling steps of oxygen occur only on the Cu surface. The special promotion effect of dioxygen for activating Cu may shed lights on tuning selectivity and activity of other transition metal catalysts.

In summary, we demonstrate oxygen-modulated catalytic performance of Cu nanowires for hydrogen evolution from aqueous solution of formaldehyde. The results show that pure metallic Cu is almost inert for formaldehyde due to the weak adsorption. Interestingly, the adsorption is strengthened by introducing oxygen

during the spontaneous reaction. The main reason is that the Cu^{+} and $O_2^{\bullet-}$ are formed on Cu surface after the oxygen injection. As a result, the molecular O_2 greatly enhances the reforming reaction rate without consumption. This hydrogen evolution reaction not only brings opportunities to the development of pure H_2 source for fuel cell, but also shines light on the special effect of oxygen in catalytic reaction.

Declaration of competing interest

The authors declare that they have no known competing financial interests or personal relationships that could have appeared to influence the work reported in this paper.

Acknowledgments

This work is supported by the China BaoWu Low Carbon Metallurgical Innovation Foundation (No. BWLCF202113), the Fundamental Research Funds for the Central Universities (Nos. N2202012, N180206004) and the National Natural Science Foundation of China (No. 51971059).

Supplementary materials

Supplementary material associated with this article can be found, in the online version, at doi:10.1016/j.cclet.2022.107905.

References

[1] V.R. Stamenkovic, D. Strmcnik, P.P. Lopes, N.M. Markovic, Nat. Mater. 16 (2017) 57–69.
[2] T. Feng, X.F. Meng, S.T. Gao, et al., Catal. Commun. 113 (2018) 10–14.
[3] A.K. Singh, S. Singh, A. Kumar, Catal. Sci. Technol. 6 (2016) 12–40.
[4] J. Huo, L. Fu, C. Zhao, C. He, Chin. Chem. Lett. 32 (2021) 2269–2273.
[5] F. Xu, X. Liu, ACS Catal. 11 (2021) 13913–13920.
[6] Q. Jin, Y. Shen, Y. Cai, L. Chu, Y. Zeng, J. Hazard. Mater. 381 (2020) 120934.
[7] J. Su, C. Cheng, Y. Guo, H. Xu, Q. Ke, J. Hazard. Mater. 380 (2019) 120890.
[8] S. Chen, S. Liang, B. Wu, et al., ACS Appl. Mater. Interfaces 11 (2019) 33946–33954.
[9] Y. Shen, Z. Xu, L. Wang, Y. Zhan, Green Chem. 23 (2021) 5618–5624.
[10] R. Li, X. Zhu, X. Yan, et al., ACS Catal. 7 (2017) 1478–1484.
[11] K. Li, J. Ji, Y. Gan, H. Huang, Chin. Chem. Lett. 33 (2022) 434–437.
[12] R. Camposeco, R. Zanella, Catal. Today 392–393 (2022) 23–30.
[13] L. Yang, J. Yang, Q. Dong, et al., J. Electroanal. Chem. 881 (2021) 114965.
[14] F. Hajilari, K. Farhadi, H. Eskandari, F. Allahnouri, Electrochim. Acta 355 (2020) 136751.
[15] S. Gong, W. Wang, K. Chen, K. Xiao, Y. Yin, J. Environ. Chem. Eng. 10 (2022) 107571.
[16] Z. Zhou, Y.H. Ng, S. Xu, et al., ACS Appl. Mater. Interfaces 13 (2021) 37299–37307.
[17] X. Chen, H. Zhang, Z. Xia, S. Zhang, Y. Ma, Catal. Sci. Technol. 9 (2019) 783–788.
[18] B. Huang, H. Kobayashi, T. Yamamoto, et al., Angew. Chem. Int. Ed. 58 (2019) 2230–2235.
[19] X. Zhu, Q. Guo, Y. Sun, et al., Nat. Commun. 10 (2019) 1428.
[20] A. Dasgupta, R.M. Rioux, Catal. Today 330 (2019) 2–15.
[21] Y. Liu, H. Chen, C. Xu, et al., Small 15 (2019) 1901789.
[22] J. Bansmann, A.M.A. Mageed, S. Chen, et al., Catalysts 9 (2019) 785.
[23] Q. Lei, H. Zhu, K. Song, et al., J. Am. Chem. Soc. 142 (2020) 4213–4222.
[24] X. Yuan, S. Chen, D. Cheng, et al., Angew. Chem. Int. Ed. 60 (2021) 15344–15347.
[25] T.C. Chou, C.C. Chang, H.L. Yu, et al., J. Am. Chem. Soc. 142 (2020) 2857–2867.
[26] G. Zhang, Z.J. Zhao, D. Cheng, et al., Nat. Commun. 12 (2021) 5745.
[27] D. Gao, R.M.A. Ais, H.S. Jeon, B.R. Cuenya, Nat. Catal. 2 (2019) 198–210.
[28] A.M.B. Gonçalves, L.C. Campos, A.S. Ferlauto, R.G. Lacerda, J. Appl. Phys. 106 (2009) 034303.
[29] M. Chen, Y. Yue, Y. Ju, J. Appl. Phys. 111 (2012) 104305.
[30] Y. Wu, M. Gao, S. Li, Y. Ren, G. Qin, Mater. Lett. 211 (2018) 247–249.
[31] X. Cao, J. Zhou, Z. Zhai, et al., ACS Sustain. Chem. Eng. 9 (2021) 3616–3623.
[32] Z. Lyu, S. Zhu, M. Xie, et al., Angew. Chem. Int. Ed. 60 (2021) 1909–1915.
[33] N. Altaf, S. Liang, L. Huang, Q. Wang, J. Energy Chem. 48 (2020) 169–180.
[34] W. Ma, S. Xie, T. Liu, et al., Nat. Catal. 3 (2020) 478–487.
[35] Y. Bi, G. Lu, Int. J. Hydrog. Energy 33 (2008) 2225–2232.
[36] A. Marimuthu, J. Zhang, S. Linic, Science 339 (2013) 1590–1593.
[37] S. Zhang, Y. Ma, H. Zhang, et al., Angew. Chem. Int. Ed. 56 (2017) 8245–8249.
[38] D. Preti, S. Squarcialupi, G. Fachinetti, Angew. Chem. Int. Ed. 48 (2009) 4763–4766.
[39] A. Soon, M. Todorova, B. Delley, C. Stampfl, Phys. Rev. B 73 (2006) 165424.
[40] H. Duan, J. Liu, M. Xu, et al., Nat. Catal. 2 (2019) 1078–1087.
[41] Z. Liu, E. Huang, I. Orozco, et al., Science 368 (2020) 513–517.
[42] S. Liang, S. Chen, Z. Guo, et al., Catal. Sci. Technol. 9 (2019) 5292–5300.
[43] S.S. Starodubov, I.V. Nechaev, A.V. Vvedenskii, Russ. J. Phys. Chem. A 90 (2016) 122–129.
[44] J.R. Gomes, J.A.N. Gomes, F. Illas, J. Mol. Catal. A Chem. 170 (2001) 187–193.
[45] L. Miao, Q. Nie, J. Wang, G. Zhang, P. Zhang, Appl. Catal. B: Environ. 248 (2019) 466–476.
[46] E. Broclawik, J. Załucka, P. Kozyra, M. Mitoraj, J. Datka, Catal. Today 169 (2011) 45–51.
[47] E.K. Zając, J. Datka, J. Phys. Chem. C 111 (2007) 3471–3475.